

Article

Investigation of Different Aqueous Electrolytes for Biomass-Derived Activated Carbon-Based Supercapacitors

Sofia Jeniffer Rajasekaran ¹, Andrews Nirmala Grace ¹, George Jacob ¹, Abdullah Alodhayb ², Saravanan Pandiaraj ² and Vimala Raghavan ^{1,*}

¹ Centre for Nanotechnology Research, Vellore Institute of Technology, Vellore 632 014, India

² Department of Physics and Astronomy, College of Science, King Saud University, P.O. Box 2455, Riyadh 11451, Saudi Arabia

* Correspondence: vimala.r@vit.ac.in

Abstract: The present work reports the synthesis of biomass derived activated carbon and its electrochemical behaviour in different electrolytes. Ricinus communis shell (RCS) was used as a raw material in this study for the synthesis of activated carbon (AC) following a high-temperature activation procedure using potassium hydroxide as the activating agent. The physical and structural characterization of the prepared Ricinus communis shell-derived activated carbon (RCS-AC) was carried by Brunauer-Emmett-Teller analysis, X-ray diffraction analysis, Fourier Transform Infrared Spectroscopy, Raman Spectroscopy and Scanning Electron Microscopy. The synthesized AC was electrochemically characterized using various techniques such as Cyclic voltammetry (CV), galvanostatic charge–discharge (GCD) tests, and Electrochemical impedance spectroscopy (EIS) measurements in different aqueous electrolytes (KOH, H₂SO₄, and Na₂SO₄). The results show that the double layer properties of the RCS-AC material in different electrolytes are distinct. In specific, the working electrode tested in 3 M KOH showed excellent electrochemical performance. It demonstrated a specific capacitance of 137 F g⁻¹ (at 1 A g⁻¹ in 3 M KOH) and exhibited high energy and power densities of 18.2 W hkg⁻¹ and 663.4 W kg⁻¹, respectively. The observed capacitance in 3 M KOH remains stable with 97.2% even after 5000 continuous charge and discharge cycles, indicating long-term stability. The study confirmed that the synthesized RCS-derived activated carbon (RCS-AC) exhibits good stability and physicochemical characteristics, making them commercially promising and appropriate for energy storage applications.

Keywords: biomass; activated carbon; aqueous electrolyte; electrode material; energy storage; supercapacitors



Citation: Rajasekaran, S.J.; Grace, A.N.; Jacob, G.; Alodhayb, A.; Pandiaraj, S.; Raghavan, V. Investigation of Different Aqueous Electrolytes for Biomass-Derived Activated Carbon-Based Supercapacitors. *Catalysts* **2023**, *13*, 286. <https://doi.org/10.3390/catal13020286>

Academic Editor: Carlo Santoro

Received: 25 November 2022

Revised: 14 January 2023

Accepted: 19 January 2023

Published: 27 January 2023



Copyright: © 2023 by the authors. Licensee MDPI, Basel, Switzerland. This article is an open access article distributed under the terms and conditions of the Creative Commons Attribution (CC BY) license (<https://creativecommons.org/licenses/by/4.0/>).

1. Introduction

A huge amount of effort has been made in the recent years to develop renewable, environmentally sustainable, affordable, and dependable energy systems. The gradual deterioration of the atmosphere and the depletion of fossil resources have drawn the attention of researchers and scientists towards the exploration of renewable energy [1–5]. There are two kinds of electrochemical devices: batteries and capacitors, both of which are promising energy storage systems. Depending on the charge management mechanisms used, all energy storage technologies have certain advantages and disadvantages. Batteries have a low power density but a high energy density, whereas traditional capacitors have a high-power density but a low energy density [6–8]. A supercapacitor (SC), also known as an electrochemical capacitor, is an intermediary between the battery and the traditional capacitor that provides significant advantages such as enhanced strength and energy flow, high reliability, flexible operating temperature, and environmental friendliness [9,10]. The energy storage process in EDLCs depends on the efficient electrostatic accumulation of charges at the electrode-electrolyte interface and during this charge-storage procedure, there

is no charge transfer. Fast redox processes involving charge transfer at the electrode and electrolyte interfaces controls the amount of energy is stored in pseudocapacitors [11,12]. The development of numerous electrode materials for supercapacitors have been reported in the literature which can be categorised as composite materials [13–17], carbon materials derived from biomass [18], conductive polymers [19], and transition metal oxide [20]. Carbon materials from biomass are frequently used in these electrode materials because of their low cost, nontoxicity, abundance of source, and long cycle life. The most frequently reported electrode material is activated carbon derived from biomass [21,22], which has been used in industrial capacitors.

Due to the wide range of electrochemical and physicochemical properties obtained depending on the precursor and activation method used, activated carbon-based materials are frequently used as electrodes [23]. Activated carbon prepared from various biomass such as human hair [24], bean dregs [25], dead neem leaves [26], tobacco rods [27], corn-stalk core [28], cassava peel [29], fungi [30], pine cone petal [31], silk [32], rice husk [33], microalgae [34], sugar cane bagasse [35], eggshell [36] etc. has been previously reported in literature. The high packing density, high surface area, higher porosity, and high chemical and physical stability of these activated carbons are some of their common characteristics [37]. The porous nature of AC materials is considered to be advantageous for supercapacitor applications, with microporous materials having a greater impact on charge transfer processes. The material's surface area and the electrolyte's stability are the main factors responsible for the high capacitance values. Electrolyte is found to be one of the most effective elements in supercapacitor performance. There are three categories of aqueous electrolytes commonly used: base, acidic, and neutral liquids. Aqueous electrolytes outperform organic-based and ionic liquid electrolytes in terms of power density while limiting energy density [38]. Electrochemical capacitors tested with aqueous electrolytes provide additional advantages over other electrolyte systems, such as low cost, high-ionic conductivity, safety, and environmental friendliness.

In neutral electrolytes, the working potential window extends above 1.2 V to 2.2 V while it is restricted to 1.2 V in acidic and basic electrolytes [39]. The protonation or deprotonation of the functional groups is what gives carbonaceous materials derived from biomass their altered surface properties in aqueous electrolytes. Despite significant advancements, some obstacles still exist, including a low energy density and a small potential window for aqueous based electrolytes.

The current work is focussed on the investigation of the effect of aqueous-based electrolytes on the capacitance performance of carbonaceous material derived from biomass. The capacitance of the material is influenced by the relationship between the average pore size of the material and the effective size of the electrolyte ion. Ricinus communis shell is used as a precursor to prepare the highly porous carbon by pre-carbonation followed by KOH activation. The prepared carbon material has a better ionic conductivity and a good specific surface area as the electrode material. It demonstrated good capacitive performance when used as supercapacitor electrode materials in aqueous electrolytes, such as 3 M KOH, 1 M H₂SO₄, and 1 M Na₂SO₄. The established relationship between carbon electrode structures and electrolyte composition will help in understanding the impact of carbonaceous electrodes derived from biomass on the storage properties of symmetric supercapacitors.

2. Results and Discussion

The structural and phase of the prepared activated carbon was investigated by XRD analysis (Figure 1a) and as observed from the figure, RCS-derived activated carbon (RCS-AC) displays diffraction intensities, indicating the predominance of amorphous structures. It is clear that there are sharp shifts of (002) peaks at around 23° and 43° corresponding to various N and O heteroatom contents. The (002) peak represents graphitic stacking originating from randomly oriented aromatic carbon. This might be due to the high temperature activation process.

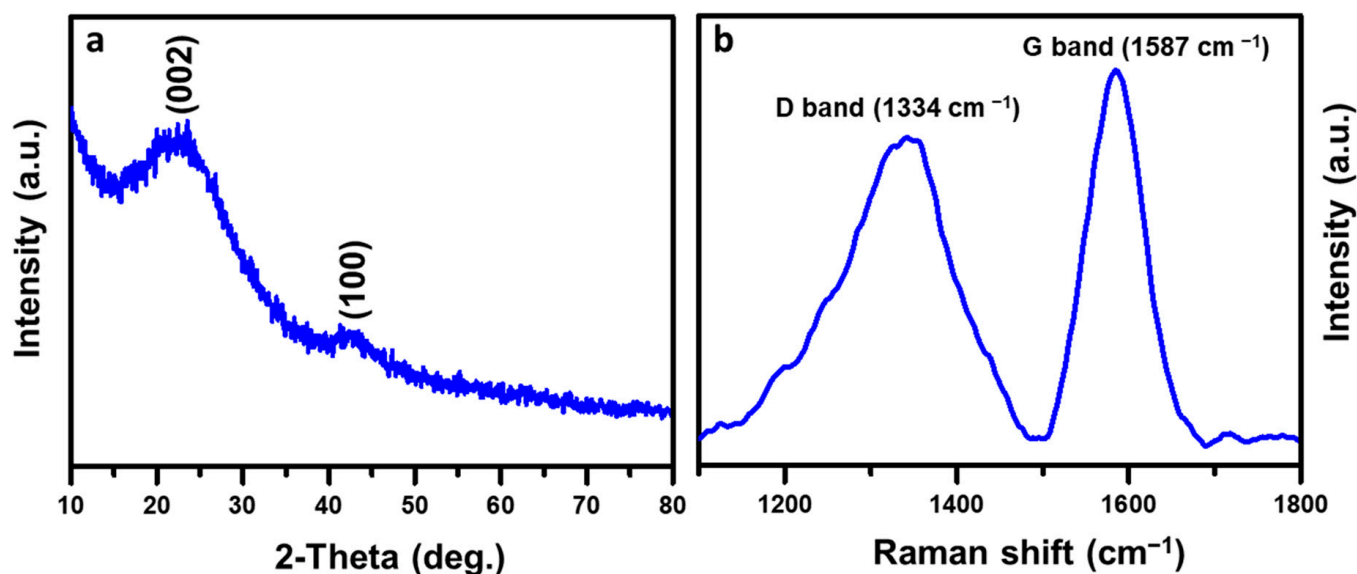


Figure 1. (a) X-Ray diffraction spectrum and (b) Raman spectrum of RCS derived activated carbon (RCS-AC).

When such high temperatures are applied, graphitic carbon structures are formed. The turbostratic or random layer lattice structure is an intermediate structure between graphite and amorphous states in the RCS-derived activated carbon [40]. Apart from the amorphous nature of RCS-derived activated carbon evident from the characteristic peaks, the D band located at 1334 cm^{-1} represents disordered and defective carbon structures, while the G band located at 1587 cm^{-1} represents the vibration of carbon atoms (Figure 1b). RCS based activated carbons with a low graphitization degree exhibits a high-intensity ratio of the D and G bands (I_D/I_G), which indicates a highly disordered characteristic nature [41]. This improves the electrode ion diffusion and electron transport abilities, as well as its surface wettability towards aqueous electrolytes. The surface functional groups in the synthesized AC were further investigated by FT-IR analysis. The spectrum of RCS derived activated carbon shows peaks at about 3325 , 1527 , 1127 , and 828 cm^{-1} (Figure 2). The peak at about 3325 cm^{-1} indicates O-H stretching vibration, while the peak at about 1527 cm^{-1} is ascribed to C=C stretching vibration. The small peaks at about 1127 cm^{-1} is attributed to C=O stretching modes, which are due to the high degrees of substitution on the C-H bond in the aromatic ring. RCS sample conductivity is enhanced by aromatization occurring during the activation and carbonization processes [42–44].

By storing charge on the surfaces via Faradaic processes, surface functional groups produce a pseudocapacitive effect that enhances capacitive behaviour. In addition to reducing charge-transfer resistance at the electrode/electrolyte interface, it increases wettability for maximum utilization of the accessible area at the electrode/electrolyte interface [45]. N_2 adsorption/desorption measurements were performed on RCS-activated carbon to determine its pore texture. According to the IUPAC classification [46], N_2 adsorption-desorption isotherm curves of all samples at 77 K have micropore and mesopore structures, as shown in Figure 3. Chemical activation of the material with KOH gives microporous and mesoporous textures. The sample exhibits high adsorption capacity at low relative pressure (0.20), indicating the presence of numerous micropores. Upon reaching $900\text{ }^\circ\text{C}$, potassium is at its boiling point and can diffuse into carbon layers, facilitating pores to form.

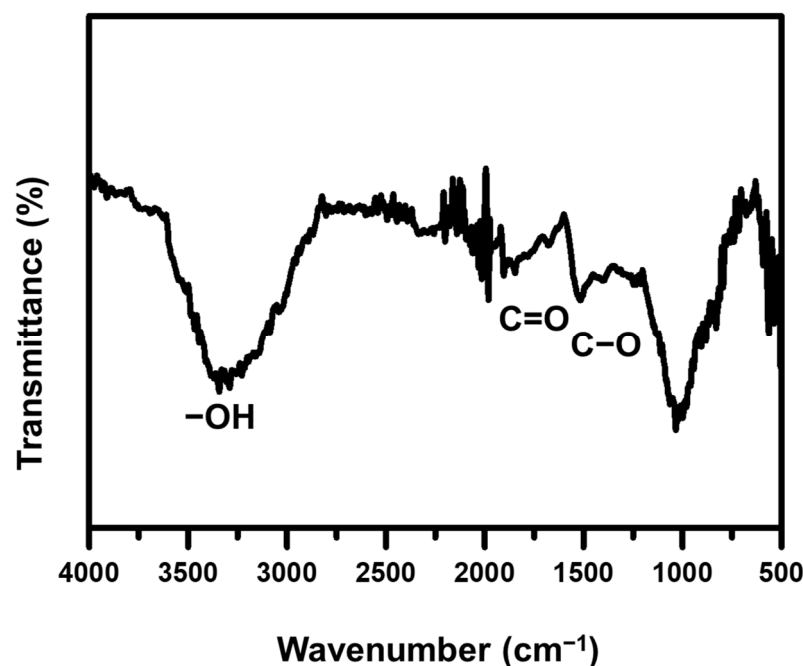


Figure 2. FT-IR spectrum of the Ricinus communis shell-derived activated carbon (RCS-AC) sample.

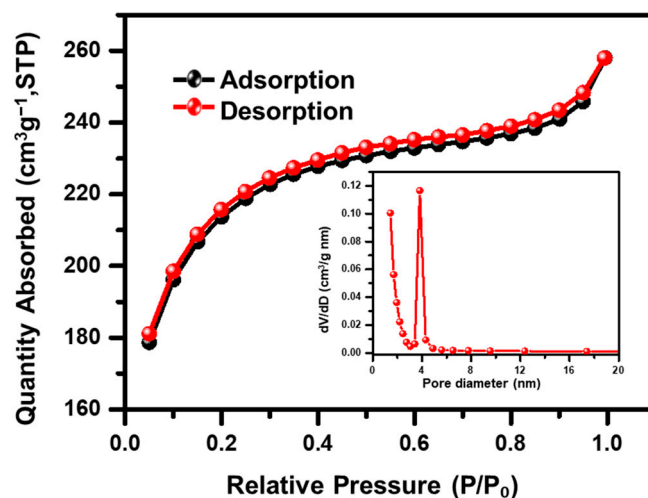


Figure 3. N₂ adsorption-desorption analysis isotherm of RCS-AC (inset shows magnified view of BJH showing pore size distribution).

Thus, higher temperatures would facilitate the formation of mesopores through enlargement or a combination of micropores. A hysteresis loop between 0.4 and 0.9 relative pressure shows mesopores, and a tail at 1.0 shows the presence of macropores. At low pressures, the N₂ uptake increases exponentially, indicating micropores while, the concave curve of the isotherm with hysteresis indicates hierarchical micro/mesoporous structures [47]. These results provide insight into how KOH contributes to microporous structures in RCS at high temperatures. As ions move from the neutral electrolyte bulk to the electrode/electrolyte interface, micropores store charges and adsorb ions, while mesopores create channels for the ions. RCS activated carbon has a specific surface area of 1917 m²g⁻¹. The inset in Figure 3 shows that RCS-AC samples have micropores and mesopores. In Barrett–Joyner–Halenda (BJH) analysis, micropores and mesopores have an average size of 3.8 nm. The porous structure and specific surface area of the AC improves ion access at high charge/discharge rates and reduces ion transport time from electrode to electrolyte, which is an important factor for achieving satisfactory power performance [48].

This study indicates that activation temperature can be used to fine-tune the material structure, which has a significant impact on the supercapacitor performance. Further to understand the morphology of RCS-AC, SEM analysis was carried out (Figure 4). During carbonization, volatile compounds were removed from the *Ricinus communis* shells, giving rise to a honeycomb structure with different pore sizes and shapes (Figure 4a,b). There is an uneven distribution of microblocks and cavities in the samples regardless of the KOH activation. As a result of the high oxidation properties of KOH and decarboxylation reactions taking place with other functional groups, small pores in the microstructure could be observed. It is evident from the results that the porosity of the activated carbon is determined by its activating agent.

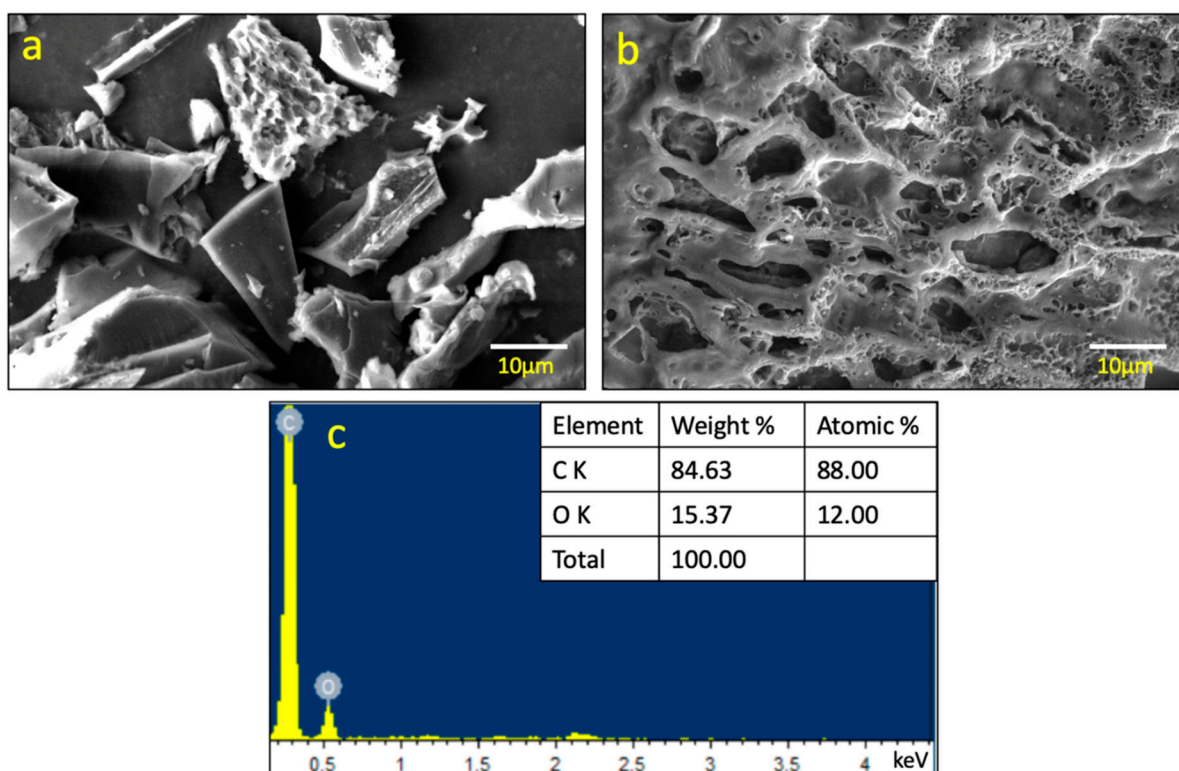


Figure 4. SEM images of (a) RCS raw material and (b) RCS-AC and (c) EDAX profile of RSC-AC prepared sample.

As observed from the images, the pores are well connected and uniform and this would facilitate the ease diffusion of electrolyte ions into the mesopores and micropores of the material. In addition, a variety of pores were seen and the majority of which were formed by KOH activation. Fast ion transport required for high-performance supercapacitors could be achieved with this kind of structure, which provides an efficient ion path during electrochemical measurements. The volume of KOH, activation temperature, and its unique reaction, in addition to the carbon source, are believed to play an important role in charge transport [49]. Furthermore, EDAX analysis was carried out to determine their chemical compositions (Figure 4c) and it could be observed that there is a high C and O content in the *Ricinus communis* shell-derived carbon, which might be due to the activation of KOH.

Further the synthesized materials were fabricated as electrode probe and further analysed for its energy storage properties via various electrochemical tests including cyclic voltammetry, galvanostatic charge discharge and impedance analysis. A three-electrode system was used to evaluate the electrochemical behaviour of the RCS-derived activated carbon with various aqueous electrolytes (acid, base, and neutral). The electrolyte study was carried out to understand the properties of the materials and its behaviour with the applied potential. Cyclic voltammetry was carried out with the electrode in KOH,

Na_2SO_4 , H_2SO_4 and given in Figure 5. As observed from the figure, KOH and Na_2SO_4 electrolytes have rectangular CV curves, while H_2SO_4 has a highly resistive CV curve due to its lower molar conductivity (Figure 5a). The difference in the electrode material behaviour may be attributed to the differences in the physical characteristics of the ions in different electrolytes. As observed from the figure, a larger current response was obtained in KOH electrolyte (Figure 5a). To obtain more accurate capacitance measurements, galvanostatic charge/discharge measurements were performed. The galvanostatic charge—discharge measurements were carried out with a three-electrode system in the potential window 0.2 V to 0.6 V to provide complementary measurements of the specific capacitances of the electrodes. Figure 5b shows a typical charge/discharge curve for the three electrolytes at current densities ranging from 1 to 10 A g^{-1} with a calculated specific capacitance of 137, 85, and 70 F g^{-1} in KOH, Na_2SO_4 , and H_2SO_4 electrolytes. In 3 M KOH electrolyte, the charge/discharge curves are almost perfect isosceles, giving a high capacitance value. The electrodes exhibit good charge/discharge behaviour and the shape of the curve shows double layer capacitance behaviour and a deviation from linearity is also observed, which is an indicative of pseudocapacitive nature of the carbon material. In general, any energy storage device should have low internal resistance as less energy is wasted as unwanted heat during the charging and discharging processes. As observed from the figure, the curves are reversible thus implying a good capacitive nature. As shown in Figure 5c, specific capacitance varies with current density.

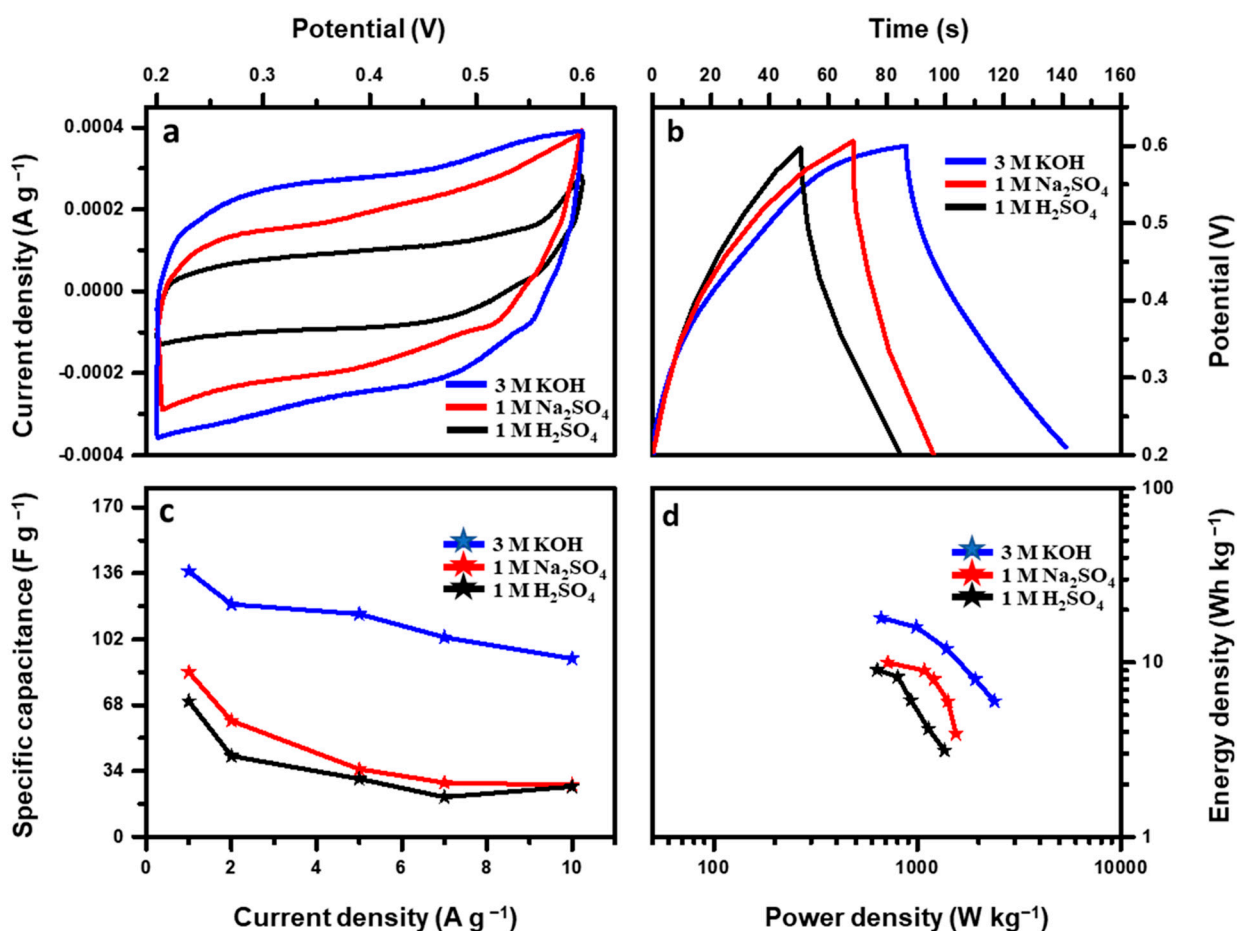


Figure 5. (a) Cyclic voltammetry curves of the electrode in different electrolytes and scan rate of 100 mVs^{-1} (b) Galvanostatic charge/discharge curves of the RCS-AC electrode at 1 A g^{-1} current density (c) Specific capacitance of the electrode as a function of current density and (d) Ragone plot of RCS-AC in different electrolytes.

Based on the molar ionic conductivity of K^+ , Na^+ and H^+ , KOH electrolyte had the highest specific capacitance, followed by Na_2SO_4 and H_2SO_4 . A high molar conductivity electrolyte will allow easy percolation of ions in the electrode material leading to a higher specific capacitance. KOH also exhibits a sustainable capacitance with increasing scan rates when compared to the other two electrolytes. The specific capacitance of a supercapacitor is determined by the pore structure of its electrode material and the degree to which its electrolyte matches its pore size [50]. The Ragone plot of activated carbon derived from RCS is given in Figure 5d, which demonstrates its energy and power density. The specific capacitance of a supercapacitor is directly proportional to its energy density. Consequently, the RCS derived activated carbon exhibits a maximum energy density of 18.2 W h kg^{-1} at 663.4 W kg^{-1} in KOH electrolyte and 6.2 W h kg^{-1} at 2420.9 W kg^{-1} . In Na_2SO_4 electrolyte, it shows a maximum energy density of 10.5 W h kg^{-1} at a power density of 715 W kg^{-1} , while in H_2SO_4 electrolyte, it shows a maximum energy density of 9.06 W h kg^{-1} at a power density of 635.6 W kg^{-1} , outperforming other ACs derived from lotus seedpods [51], chicken feathers [52], corn husks [53], 3D flowerlike carbon [54], jujube pits [55], waste tea leaves [56]. Performance comparison of activated carbon derived from different biomass is given in Table 1.

Table 1. Performance comparison of activated carbon derived from different biomass.

Biomass	Activating Agent	Specific Capacitance ($F \text{ g}^{-1}$)	Energy Density (ED) ($W \text{ h kg}^{-1}$)	Power Density (PD) ($W \text{ kg}^{-1}$)	Current Density	Electrolyte	Reference
Rotten carrot	$ZnCl_2$	135	29.1	142.5	1 mA cm^{-2}	KOH	Ahmed et al., 2018 [57]
Banana peel waste	-	68	0.75	31	-	H_2SO_4	Taer et al., 2017 [58]
Loofah sponge	KOH	78.2	34.7	26.8	1 A g^{-1}	Na_2SO_4	Luan et al., 2016 [59]
Pinecone	KOH + CO_2	137	19	100	0.1 A g^{-1}	Na_2SO_4	Barzegar et al., 2017 [60]
Cow dung	KOH	124	28	-	1 A g^{-1}	Et_4NBF_4	Bhattacharjya and Yu, 2014 [61]
Pine biomass	KOH	69	24.6	400	0.5 A g^{-1}	KOH/PVA	Bello et al., 2016 [62]
Sugarcane Bagasse	KOH	142	19.74	0.5	0.5 A g^{-1}	KOH	Hao et al., 2014 [63]
Ricinus communis shell	KOH	137	18.2	663.4	1 A g^{-1}	KOH	Present work

At higher charge/discharge rates, the impedance and diffusion routes in the pore structure are related to energy and power limitations. Only a portion of the porous structure can absorb electrolyte ions at high diffusion currents, whereas both the medial and lateral porous structures can absorb charge at lower diffusion currents [64]. Therefore, the aqueous-based electrolyte viz. KOH has the potential to increase the energy density of aqueous symmetric RCS-derived activated carbon and is also an ideal carbon material with high capacitance.

It is also important to consider the cycle life of supercapacitors. In Figure 6a, galvanostatic charge/discharge measurements were used to evaluate the long-term cyclic stability of capacitance performance with acidic, basic and neutral electrolytes. Cyclic stability of 97.2%, 93.6% and 84.8% was achieved for the electrolytes KOH, Na_2SO_4 and H_2SO_4 at 5000 cycles. KOH electrolyte demonstrates good cyclic charge and discharge performance for activated carbon derived from RCS. The increased stability of the electrode material may be attributed to the presence of surface carbonyl and oxygen functional groups in the RCS derived activated carbon, which may cause redox reactions with KOH electrolyte. As a result, it is evident that the activated carbon derived from *Ricinus communis* shell is electrochemically stable with long-term cycle life.

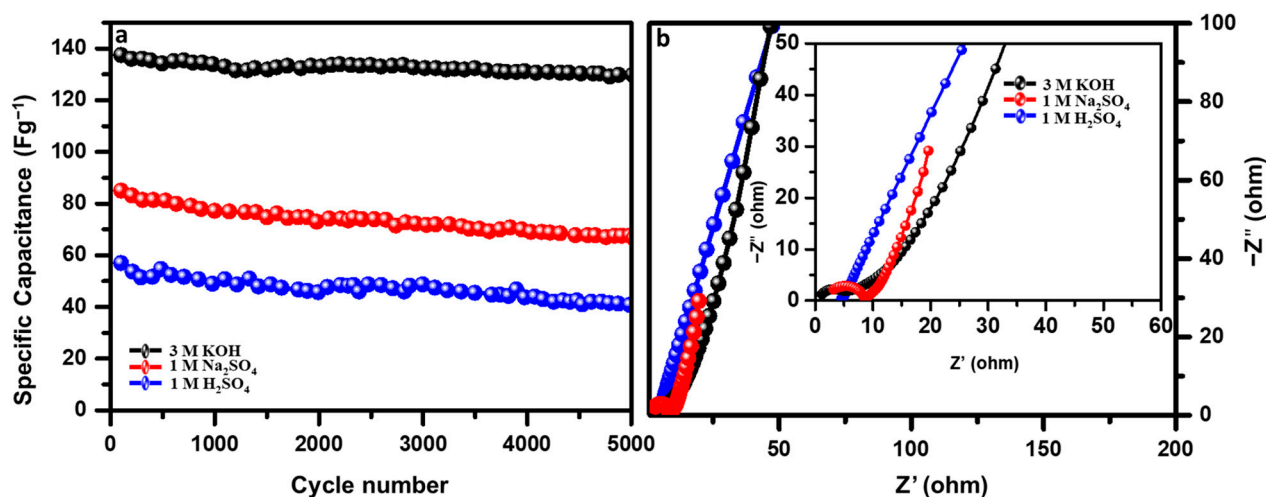


Figure 6. (a) Cyclic stability of RCS derived activated carbon electrode up to 5000 cycles (b) Nyquist plots of the electrode in different electrolytes (Inset—An expanded representation of the EIS plot in the high-frequency region).

Figure 6b shows the Nyquist plots of RCS-AC from EIS measurements in different electrolytes in the frequency range of 100 kHz to 10 MHz. The observed spectra show different behaviours in three different frequency regions. All the electrolyte capacitive behaviour can be approximated by almost vertical lines in the low-frequency region. In the zoomed region (inset of Figure 6b), a semicircle can be seen indicating the presence of resistance in the electrode. The porous nature of the electrode and the existence of resistance at the electrode-electrolyte interface is the primary cause of the observed semicircle.

At the electrode-electrolyte interface, a wide semicircle indicates resistance dominance, while a smaller semicircle suggests capacitive dominance. As it is a transition range between the low frequency (right angles zone) and high-frequency ranges, this range is also known as the “knee” region (Warburg region). The “knee” is the transition point between the high and low-frequency ranges. The frequency at the knee is a measure of a supercapacitors rate capability since it represents the maximum frequency at which the capacitive characteristic is dominant [65]. Further, the width of the impedance arc at this transition area denotes resistance due to ion diffusion and transportation at the electrode/electrolytes interface. The ESR of the RCS-AC electrode is approximated at $\sim 1.1 \Omega$ for KOH electrolyte and 3.1Ω and 4.5Ω for Na_2SO_4 and H_2SO_4 electrolytes, respectively. Low ESR values indicate low internal resistance within the material, cell components, electrolyte and current collector which further qualifies for electrode application. The as-prepared RCS derived activated carbon sample delivers a specific capacitance of 137 F g^{-1} in 3 M KOH at 1 A g^{-1} and excellent cyclic stability with a good energy density of 18.2 W h kg^{-1} at a power density of 663.4 W kg^{-1} . Table 2 shows the summary of the electrochemical parameters of RCS-AC in different electrolytes.

Table 2. Electrochemical parameters of RCS-900 in different aqueous electrolytes.

Electrolytes	Specific Capacitance (F g^{-1})	Energy Density (ED) (W h kg^{-1})	Power Density (PD) (W kg^{-1})	ESR (Ωcm^2)	Capacitance Retention (%)
KOH	137	18.2	663.4	1.1	97.2
Na_2SO_4	70	10.5	715.2	3.1	84.8
H_2SO_4	85	9.06	635.6	4.5	93.6

Further to understand the practicality of the fabricated electrode with a two-electrode system and a broad operating voltage, the CV tests were performed from 0.0 to 1.8 V vs. Ag/AgCl (Figure 7a). The curves were rectangular shaped and shows that the electrode is

beneficial for charge storage. Further the galvanostatic charge discharge curves recorded at 1 A g^{-1} current density showed that the curves were symmetric with a calculated specific capacitance of 115 F g^{-1} . These results suggest that the symmetric cell has very good electrochemical reversibility and possesses ideal capacitive nature.

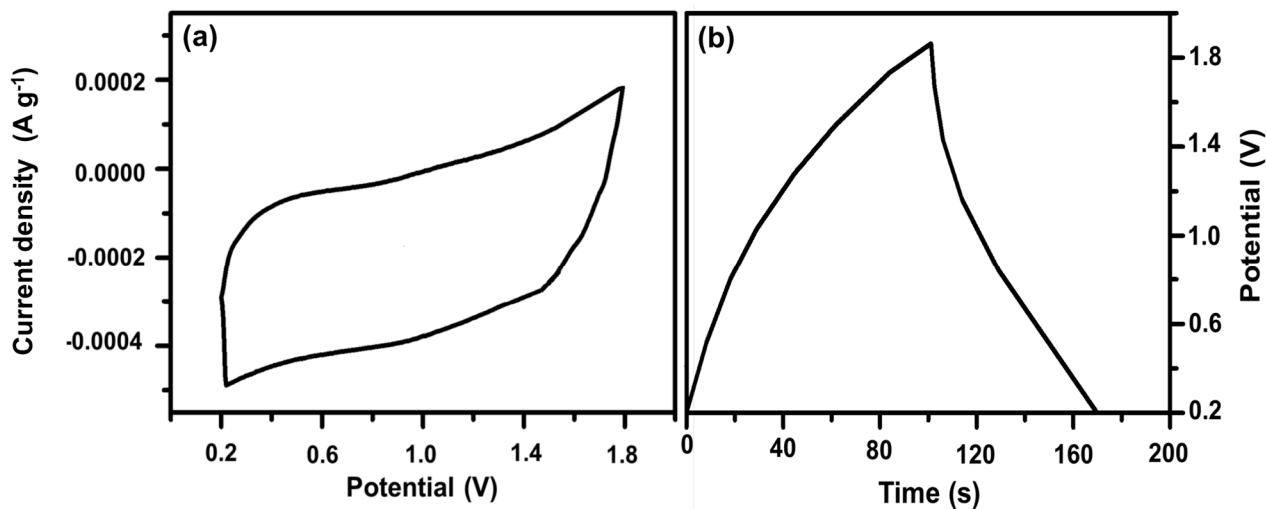


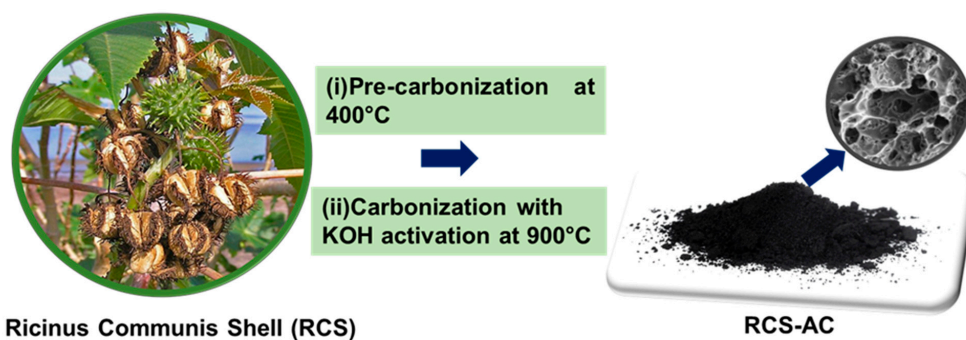
Figure 7. (a) Cyclic voltammetry curves of the electrode in 3 M KOH at a scan rate of 100 mVs^{-1} (b) Galvanostatic charge/discharge curves of the RCS-AC electrode at 1 A g^{-1} current density (Two electrode system).

Thus, an aqueous-based electrolyte to fabricate a high-energy symmetric supercapacitor with KOH-activated biomass carbon is reported to have a good capacitance and energy density, thereby making it as a promising electrode material for energy storage.

3. Experimental Section

3.1. Preparation of RCS Derived Activated Carbon (RCS-AC)

Ricinus communis shell (RCS), used for the preparation of activated carbon in this study was collected from a local agricultural farm in Coimbatore, Tamil Nadu, India. The transformation of Ricinus communis shell into activated carbon is depicted in Scheme 1. Pre-carbonization and KOH activation were combined to prepare Ricinus communis shell-based carbons. Carbonization of Ricinus communis shell was carried out in N_2 atmosphere in a horizontal tube furnace at $400 \text{ }^\circ\text{C}$ for 3 h. This was followed by KOH chemical activation of the carbonized Ricinus communis shell carbon. The porous carbon materials were obtained by mixing RCS carbon and KOH pellets in a weight ratio of 1:1 and heating at $900 \text{ }^\circ\text{C}$ under a N_2 atmosphere for one hour at a rate of $5 \text{ }^\circ\text{C}/\text{min}$. After cooling it to room temperature, it was washed with 5% HCl solution followed by thorough washing with deionized water. The resultant product is designated as RCS-AC.



Scheme 1. A schematic representation of the preparation of RCS-derived activated carbon (RCS-AC).

3.2. Physicochemical Characterization

The structure of RCS-AC was analysed using powder X-ray Diffractometer (XRD BRUKER, D8 ADVANCE, Billerica, MA, USA) with Cu K α radiation ($\lambda = 1.5418 \text{ \AA}$). The degree of graphitization of the biomass-derived activated carbon was determined using Raman spectroscopy (HORIBA Jobin Yvon LabRAM ARAMIS, Kyoto, Japan) excited at 633 nm laser. To characterize the surface chemistry, FT-IR spectra were recorded on a Fourier Transform Infrared spectrometer (IR Affinity-1, Shimadzu, Kyoto, Japan). Carbon and oxygen contents of the samples were also determined by EDX using the ZEISS Neon 40 Energy-Dispersive X-ray analyser. The morphology of the activated carbon was studied using Scanning Electron Microscopy (SEM) (ZEISS Neon 40, Jena, Germany. A Quantachrome Autosorb iQ, Odelzhausen, Germany) was used to determine porous textural properties. Brunauer–Emmett–Teller (BET) surface area and pore structure was calculated by using ASiQwin's multi-point BET-plot calculation.

3.3. Electrochemical Measurements and Electrode Preparation

To prepare the electrode the active material (RCS-AC), carbon black and PVDF binder were used in the weight ratio of 85:10:5 and then mixed, ground, and dispersed in N-methyl pyrrolidone (NMP) solution. The obtained mixture was coated on a graphite foil substrate (1 cm^2) and subjected to drying in an oven at $80 \text{ }^\circ\text{C}$ for 12 h. The prepared activated carbon was tested for its performance as supercapacitor electrode material using a three-electrode system. A CHI660C electrochemical workstation (Austin, TX, USA) was used for the electrochemical analysis including cyclic voltammetry (CV), galvanostatic charge/discharge (GCD) testing and electrochemical impedance spectroscopy (EIS). In the above technique, activated carbon was used as the working electrode, Ag/AgCl as the reference electrode, and platinum wire as the counter electrode in different electrolytes viz. 3 M KOH, 1 M Na $_2$ SO $_4$ and 1 M H $_2$ SO $_4$. Various electrochemical tests were carried out viz. cyclic voltammetry (CV), galvanostatic charge/discharge (GCD) and electrochemical impedance spectroscopy (EIS) techniques in the frequency range from 100 kHz to 0.1 Hz and an amplitude of 5 mV. The specific capacitance of an electrode material was calculated using the equation given below [66]:

$$C_s = \frac{I \times \Delta t}{m \times \Delta v} \quad (1)$$

where C_s represents the specific capacitance at constant current in F g^{-1} , mass (m), discharge time (t) and potential window (V). With the three-electrode system, the galvanostatic charge/discharge measurement was used to calculate the energy density (E) and power density (P) [67]:

$$E = \frac{1}{2} C_s (\Delta V)^2 \quad (2)$$

$$P = \frac{E}{\Delta t} \quad (3)$$

where C_s , ΔV and Δt are the specific capacitance, discharge cell voltage window and discharging time (s), respectively. For the two-electrode system, two symmetrical electrodes, each measuring $15 \times 15 \text{ mm}^2$ were prepared following the same procedure. A glass fibre separator was used between the two electrodes and the electrode was soaked in 3 M KOH electrolyte. A two-electrode measurement was carried out to understand the practicality of the fabricated electrode and the electrochemical investigation was carried out in 3 M KOH in a cell type symmetric device. Initially CV tests were carried out to verify the operating voltage range of the fabricated device.

4. Conclusions

The work reports the development of activated carbon material for supercapacitors from *Ricinus communis* shell biomass. Porous RCS-derived activated carbon was synthe-

sized through a combination of pre-carbonization and KOH activation. The surface morphology, crystalline structure, and vibrational response of the synthesized RCS-AC were investigated using standard material characterization techniques. The synthesized RCS derived activated carbon was evaluated for supercapacitors in different aqueous electrolytes. The electrochemical behaviour was investigated using cyclic voltammetry, galvanostatic charge/discharge and electrochemical impedance spectroscopy in various electrolytes viz. 3 M KOH, 1 M Na₂SO₄ and 1 M H₂SO₄. With a power density of 663.4 W hkg⁻¹ and a maximum energy density of 18.2 W hkg⁻¹, the RCS derived activated electrode material showed good electrochemical storage capabilities in 3 M KOH. At various current densities, the electrode was more efficient at charging and discharging in 3 M KOH electrolyte compared to 1 M Na₂SO₄ and 1 M H₂SO₄. The electrode delivered an excellent specific capacitance and long cyclic life in KOH. The observations from this study reveal that the as-prepared Ricinus communis shell derived activated carbon could make a significant influence in the production of low-cost efficient electrode material for supercapacitors.

Author Contributions: Conceptualization, A.N.G.; Methodology, S.J.R.; Software, S.J.R.; Validation, G.J. and V.R.; Formal analysis, A.N.G. and G.J.; Investigation, S.J.R.; Resources, A.N.G. and V.R.; Data curation, G.J.; Writing—original draft preparation, S.J.R.; Writing—review and editing, A.A. and S.P.; Visualization, A.A. and S.P.; Supervision, A.N.G. and V.R.; Project administration, Funding acquisition, A.A. and S.P. All authors have read and agreed to the published version of the manuscript.

Funding: This research was funded by Researchers Supporting Project number (RSP2023R304), King Saud University, Riyadh, Saudi Arabia.

Data Availability Statement: Data available on request.

Acknowledgments: The authors are thankful to the Vellore Institute of Technology, Vellore for providing the facilities to carry out this research work. Author Abdullah Alodhayb acknowledges Researchers Supporting Project number (RSP2023R304), King Saud University, Riyadh, Saudi Arabia.

Conflicts of Interest: The authors declare no conflict of interest.

References

1. Fu, K.K.; Cheng, J.; Li, T.; Hu, L. Flexible Batteries: From Mechanics to Devices. *ACS Energy Lett.* **2016**, *1*, 1065–1079. [[CrossRef](#)]
2. Fan, L.; Jia, C.; Zhu, Y.G.; Wang, Q. Redox targeting of Prussian blue: Toward low-cost and high energy density redox flow battery and solar rechargeable battery. *ACS Energy Lett.* **2017**, *2*, 615–621. [[CrossRef](#)]
3. Kumar, J.C.R.; Majid, M.A. Renewable energy for sustainable development in India: Current status, prospects, challenges, employment, and investment opportunities. *Energy Sustain. Soc.* **2020**, *10*, 1–36. [[CrossRef](#)]
4. Elemans, J.; Rowan, A.; Nolte, R.J.M. Mastering molecular matter. Supramolecular architectures by hierarchical self-assembly. *J. Mater. Chem.* **2003**, *13*, 2661–2670. [[CrossRef](#)]
5. Whitesides, G.M.; Mathias, J.P.; Seto, C.T. Molecular self-assembly and nanochemistry: A chemical strategy for the synthesis of nanostructures. *Science* **1991**, *254*, 1312–1319. [[CrossRef](#)] [[PubMed](#)]
6. AL Shaqsi, A.Z.; Sopian, K.; Al-Hinai, A. Review of energy storage services, applications, limitations, and benefits. *Energy Rep.* **2020**, *6*, 288–306. [[CrossRef](#)]
7. Riaz, A.; Sarker, M.; Saad, M.; Mohamed, R. Review on comparison of different energy storage technologies used in micro-energy harvesting, wins, low-cost microelectronic devices: Challenges and recommendations. *Sensors* **2021**, *21*, 5041. [[CrossRef](#)]
8. Jalal, N.I.; Ibrahim, R.I.; Oudah, M.K. A review on Supercapacitors: Types and components. *J. Phys. Conf. Ser.* **2021**, *1973*, 012015. [[CrossRef](#)]
9. Shao, H.; Wu, Y.-C.; Lin, Z.; Taberna, P.-L.; Simon, P. Nanoporous carbon for electrochemical capacitive energy storage. *Chem. Soc. Rev.* **2020**, *49*, 3005–3039. [[CrossRef](#)] [[PubMed](#)]
10. Guo, Y.; Wang, Y.; Zhang, Y.; Zhai, Y.; Cai, W. Functional sulfur-doped zinc-nickel-cobalt oxide nanorods materials with high energy density for asymmetric supercapacitors. *J. Alloys Compd.* **2022**, *896*, 163053. [[CrossRef](#)]
11. Ranganatha, S. 2D Nanostructured Materials for High-Performance Electrochemical Supercapacitors. *ACS Symp. Ser.* **2020**, *1353*, 79–92. [[CrossRef](#)]
12. Liu, J.; Wang, J.; Xu, C.; Jiang, H.; Li, C.; Zhang, L.; Lin, J.; Shen, Z.X. Advanced Energy Storage Devices: Basic Principles, Analytical Methods, and Rational Materials Design. *Adv. Sci.* **2018**, *5*, 1700322. [[CrossRef](#)] [[PubMed](#)]
13. Wu, D.; Xie, X.; Zhang, Y.; Zhang, D.; Du, W.; Zhang, X.; Wang, B. MnO₂/Carbon Composites for Supercapacitor: Synthesis and Electrochemical Performance. *Front. Mater.* **2020**, *7*, 2. [[CrossRef](#)]
14. Hassan, H.; Iqbal, M.W.; Afzal, A.M.; Asghar, M.; Aftab, S. Enhanced the performance of zinc strontium sulfide-based supercapacitor device with the polyaniline doped activated carbon. *J. Solid State Electrochem.* **2022**, *27*, 125–137. [[CrossRef](#)]

15. Afzal, A.M.; Ali, M.; Iqbal, M.W.; Imran, M.; Rehman, A.U.; Mumtaz, S.; Kim, J.S.; Choi, E.H.; Alanazi, Y.M. Enhanced the electrochemical performance and stability of supercapattery device with carbon nanotube/cobalt-manganese sulfide-based composite electrode material. *Int. J. Energy Res.* **2022**, *46*, 24355–24367. [[CrossRef](#)]
16. Zaka, A.; Iqbal, M.W.; Afzal, A.M.; Hassan, H.; Alzahrani, H.A.; Yasmeen, A.; Abbas, T.; Aftab, S.; Neffati, R. Facile synthesis of strontium copper phosphate (SrCuPO₄) binary composite for the high-performance supercapattery devices. *J. Mater. Sci. Mater. Electron.* **2022**, *33*, 27002–27013. [[CrossRef](#)]
17. Ali, M.; Afzal, A.M.; Iqbal, M.W.; Mumtaz, S.; Imran, M.; Ashraf, F.; Rehman, A.U.; Muhammad, F. 2D-TMDs based electrode material for supercapacitor applications. *Int. J. Energy Res.* **2022**, *46*, 22336–22364. [[CrossRef](#)]
18. Rajasekaran, S.J.; Raghavan, V. Facile synthesis of activated carbon derived from Eucalyptus globulus seed as efficient electrode material for supercapacitors. *Diam. Relat. Mater.* **2020**, *109*, 108038. [[CrossRef](#)]
19. Snook, G.A.; Kao, P.; Best, A.S. Conducting-polymer-based supercapacitor devices and electrodes. *J. Power Sources* **2011**, *196*, 1–12. [[CrossRef](#)]
20. Liang, R.; Du, Y.; Xiao, P.; Cheng, J.; Yuan, S.; Chen, Y.; Yuan, J.; Chen, J. Transition metal oxide electrode materials for supercapacitors: A review of recent developments. *Nanomaterials* **2021**, *11*, 1248. [[CrossRef](#)]
21. Ghosh, S.; Santhosh, R.; Jeniffer, S.; Raghavan, V.; Jacob, G.; Nanaji, K.; Kollu, P.; Jeong, S.K.; Grace, A.N. Natural biomass-derived hard carbon and activated carbons as electrochemical supercapacitor electrodes. *Sci. Rep.* **2019**, *9*, 16315. [[CrossRef](#)] [[PubMed](#)]
22. Kim, J.-H.; Lee, H.-M.; Jung, S.-C.; Chung, D.-C.; Kim, B.-J. Bamboo-based mesoporous activated carbon for high-power-density electric double-layer capacitors. *Nanomaterials* **2021**, *11*, 2750. [[CrossRef](#)] [[PubMed](#)]
23. Gan, Y.X. Activated Carbon from Biomass Sustainable Sources. *C* **2021**, *7*, 39. [[CrossRef](#)]
24. Qian, W.; Sun, F.; Xu, Y.; Qiu, L.; Liu, C.; Wang, S.; Yan, F. Human hair-derived carbon flakes for electrochemical supercapacitors. *Energy Environ. Sci.* **2014**, *7*, 379–386. [[CrossRef](#)]
25. Ruan, C.; Ai, K.; Lu, L. Biomass-derived carbon materials for high-performance supercapacitor electrodes. *RSC Adv.* **2014**, *4*, 30887–30895. [[CrossRef](#)]
26. Biswal, M.; Banerjee, A.; Deo, M.; Ogale, S. From dead leaves to high energy density supercapacitors. *Energy Environ. Sci.* **2013**, *6*, 1249–1259. [[CrossRef](#)]
27. Zhao, Y.-Q.; Lu, M.; Tao, P.-Y.; Zhang, Y.-J.; Gong, X.-T.; Yang, Z.; Zhang, G.-Q.; Li, H.-L. Hierarchically porous and heteroatom doped carbon derived from tobacco rods for supercapacitors. *J. Power Sources* **2016**, *307*, 391–400. [[CrossRef](#)]
28. Liu, C.; Han, G.; Chang, Y.; Xiao, Y.; Li, M.; Zhou, W.; Fu, D.; Hou, W. Properties of Porous Carbon Derived from Cornstalk Core in High-Performance Electrochemical Capacitors. *ChemElectroChem* **2016**, *3*, 323–331. [[CrossRef](#)]
29. Ismanto, A.E.; Wang, S.; Soetaredjo, F.E.; Ismadji, S. Preparation of capacitor's electrode from cassava peel waste. *Bioresour. Technol.* **2010**, *101*, 3534–3540. [[CrossRef](#)]
30. Zhu, H.; Wang, X.; Yang, F.; Yang, X. Promising carbons for supercapacitors derived from fungi. *Adv. Mater.* **2011**, *23*, 2745–2748. [[CrossRef](#)]
31. Karthikeyan, K.; Amaresh, S.; Lee, S.N.; Sun, X.; Aravindan, V.; Lee, Y.-G.; Lee, Y.S. Construction of high-energy-density supercapacitors from pine-cone-derived high-surface-area carbons. *ChemSusChem* **2014**, *7*, 1435–1442. [[CrossRef](#)] [[PubMed](#)]
32. Hou, J.; Cao, C.; Idrees, F.; Ma, X. Hierarchical porous nitrogen-doped carbon nanosheets derived from silk for ultrahigh-capacity battery anodes and supercapacitors. *ACS Nano* **2015**, *9*, 2556–2564. [[CrossRef](#)] [[PubMed](#)]
33. He, X.; Ling, P.; Qiu, J.; Yu, M.; Zhang, X.; Yu, C.; Zheng, M. Efficient preparation of biomass-based mesoporous carbons for supercapacitors with both high energy density and high power density. *J. Power Sources* **2013**, *40*, 109–113. [[CrossRef](#)]
34. Sevilla, M.; Gu, W.; Falco, C.; Titirici, M.; Fuertes, A.; Yushin, G. Hydrothermal synthesis of microalgae-derived microporous carbons for electrochemical capacitors. *J. Power Sources* **2014**, *267*, 26–32. [[CrossRef](#)]
35. Rufford, T.E.; Hulicova-Jurcakova, D.; Khosla, K.; Zhu, Z.; Lu, G.Q. Microstructure and electrochemical double-layer capacitance of carbon electrodes prepared by zinc chloride activation of sugar cane bagasse. *J. Power Sources* **2010**, *195*, 912–918. [[CrossRef](#)]
36. Li, Z.; Zhang, L.; Amirkhiz, B.S.; Tan, X.; Xu, Z.; Wang, H.; Olsen, B.; Holt, C.M.B.; Mitlin, D. Carbonized chicken eggshell membranes with 3D architectures as high-performance electrode materials for supercapacitors. *Adv. Energy Mater.* **2012**, *2*, 431–437. [[CrossRef](#)]
37. Saleem, J.; Shahid, U.B.; Hijab, M.; Mackey, H.; McKay, G. Production and applications of activated carbons as adsorbents from olive stones. *Biomass. Convers. Biorefinery* **2019**, *9*, 775–802. [[CrossRef](#)]
38. Zhong, C.; Deng, Y.; Hu, W.; Qiao, J.; Zhang, L.; Zhang, J. A review of electrolyte materials and compositions for electrochemical supercapacitors. *Chem. Soc. Rev.* **2015**, *44*, 7484–7539. [[CrossRef](#)] [[PubMed](#)]
39. Zhao, X.; Wang, Y.; Shi, Y.; Yan, X.; Tian, Y.; Zuo, Z.; Yang, X. Exploiting Interfacial Cl⁻/ClO₂Redox for a 1.8-V Voltage Plateau Aqueous Electrochemical Capacitor. *ACS Energy Lett.* **2021**, *6*, 1134–1140. [[CrossRef](#)]
40. Manoj, B.; Kunjomana, A.G. Study of stacking structure of amorphous carbon by X-ray diffraction technique. *Int. J. Electrochem. Sci.* **2012**, *7*, 3127–3134.
41. Mallick, A.K.; Jha, A.; Pokharel, B.P.; Rajbhandari, R.; Shrestha, R.M. Activated Carbons Derived from Date (Phoenix dactylifera) Seeds with Excellent Iodine Adsorption Properties. *J. Inst. Eng.* **2019**, *15*, 165–170. [[CrossRef](#)]
42. Maulina, W.; Kusumaningtyas, R.; Rachmawati, Z.; Supriyadi; Arkundato, A.; Rohman, L.; Purwandari, E. Carbonization Process of Water Hyacinth as an Alternative Renewable Energy Material for Biomass Cook Stoves Applications. *IOP Conf. Ser. Earth Environ. Sci.* **2019**, *239*, 012035. [[CrossRef](#)]

43. Zhang, L.; Tu, L.-Y.; Liang, Y.; Chen, Q.; Li, Z.-S.; Li, C.-H.; Wang, Z.-H.; Li, W. Coconut-based activated carbon fibers for efficient adsorption of various organic dyes. *RSC Adv.* **2018**, *8*, 42280–42291. [[CrossRef](#)] [[PubMed](#)]
44. Hadi, S.; Taheri, E.; Amin, M.M.; Fatehizadeh, A.; Aminabhavi, T.M. Adsorption of 4-chlorophenol by magnetized activated carbon from pomegranate husk using dual-stage chemical activation. *Chemosphere* **2021**, *270*, 128623. [[CrossRef](#)] [[PubMed](#)]
45. Wu, Z.; Li, L.; Yan, J.-M.; Zhang, X.-B. Materials Design and System Construction for Conventional and New-Concept Supercapacitors. *Adv. Sci.* **2017**, *4*, 1600382. [[CrossRef](#)]
46. Wacharasindhu, S.; Chaichanwatanakul, K.; Likitmaskul, S.; Angsusingha, K.; Punnakanta, L.; Tuchinda, C. Serum IGF-I and IGFBP-3 Levels for Normal Thai Children and their Usefulness in Clinical Practice. *J. Med. Assoc. Thail.* **1998**, *81*, 420–430.
47. Fang, Y.; Zhang, Q.; Cui, L. Recent progress of mesoporous materials for high-performance supercapacitors. *Microporous Mesoporous Mater.* **2021**, *314*, 110870. [[CrossRef](#)]
48. Subramanyan, K.; Divya, M.L.; Aravindan, V. Dual-carbon Na-ion capacitors: Progress and prospects. *J. Mater. Chem A* **2021**, *9*, 9431–9450. [[CrossRef](#)]
49. Siddique, A.B.; Morrison, K.; Venkat, G.; Pramanick, A.K.; Banerjee, N.; Ray, M. Charge Transport through Functionalized Graphene Quantum Dots Embedded in a Polyaniline Matrix. *ACS Appl. Electron. Mater.* **2021**, *3*, 1437–1446. [[CrossRef](#)]
50. Deng, J.; Li, J.; Song, S.; Zhou, Y.; Li, L. Electrolyte-dependent supercapacitor performance on nitrogen-doped porous bio-carbon from gelatin. *Nanomaterials* **2020**, *10*, 353. [[CrossRef](#)]
51. Liu, B.; Zhou, X.; Chen, H.; Liu, Y.; Li, H. Promising porous carbons derived from lotus seedpods with outstanding super capacitance performance. *Electrochim. Acta* **2016**, *208*, 55–63. [[CrossRef](#)]
52. Wang, Q.; Cao, Q.; Wang, X.; Jing, B.; Kuang, H.; Zhou, L. A high-capacity carbon prepared from renewable chicken feather biopolymer for supercapacitors. *J. Power Sources* **2013**, *225*, 101–107. [[CrossRef](#)]
53. Song, S.; Ma, F.; Wu, G.; Ma, D.; Geng, W.; Wan, J. Facile self-templating large scale preparation of biomass-derived 3D hierarchical porous carbon for advanced supercapacitors. *J. Mater. Chem A* **2015**, *3*, 18154–18162. [[CrossRef](#)]
54. Wang, Q.; Yan, J.; Wang, Y.; Wei, T.; Zhang, M.; Jing, X.; Fan, Z. Three-dimensional flower-like and hierarchical porous carbon materials as high-rate performance electrodes for supercapacitors. *Carbon* **2014**, *67*, 119–127. [[CrossRef](#)]
55. Sun, K.; Yu, S.; Hu, Z.; Li, Z.; Lei, G.; Xiao, Q.; Ding, Y. Oxygen-containing hierarchically porous carbon materials derived from wild jujube pit for high-performance supercapacitor. *Electrochim. Acta* **2017**, *231*, 417–428. [[CrossRef](#)]
56. Ma, G.; Li, J.; Sun, K.; Peng, H.; Feng, E.; Lei, Z. Tea-leaves based nitrogen-doped porous carbons for high-performance supercapacitors electrode. *J. Solid State Electrochem.* **2017**, *21*, 525–535. [[CrossRef](#)]
57. Ahmed, S.; Ahmed, A.; Rafat, M. Supercapacitor performance of activated carbon derived from rotten carrot in aqueous, organic and ionic liquid based electrolytes. *J. Saudi Chem. Soc.* **2018**, *22*, 993–1002. [[CrossRef](#)]
58. Taer, E.; Taslim, R.; Aini, Z.; Hartati, S.D.; Mustika, W.S. Activated carbon electrode from banana-peel waste for supercapacitor applications. *AIP Conf. Proc.* **2017**, *1801*, 040004. [[CrossRef](#)]
59. Luan, Y.; Huang, Y.; Wang, L.; Li, M.; Wang, R.; Jiang, B. Porous carbon@MnO₂ and nitrogen-doped porous carbon from carbonized loofah sponge for asymmetric supercapacitor with high energy and power density. *J. Electroanal. Chem.* **2016**, *763*, 90–96. [[CrossRef](#)]
60. Barzegar, F.; Bello, A.; Dangbegnon, J.K.; Manyala, N.; Xia, X. Asymmetric supercapacitor based on activated expanded graphite and pinecone tree activated carbon with excellent stability. *Appl. Energy* **2017**, *207*, 417–426. [[CrossRef](#)]
61. Bhattacharjya, D.; Yu, J.-S. Activated carbon made from cow dung as electrode material for electrochemical double layer capacitor. *J. Power Sources* **2014**, *262*, 224e231. [[CrossRef](#)]
62. Bello, A.; Manyala, N.; Barzegar, F.; Khaleed, A.A.; Momodu, D.Y.; Dangbegnon, J.K. Renewable pine cone biomass derived carbon materials for supercapacitor application. *RSC Adv.* **2016**, *6*, 1800–1809. [[CrossRef](#)]
63. Hao, P.; Zhao, Z.; Tian, J.; Li, H.; Sang, Y.; Yu, G.; Cai, H.; Liu, H.; Wong, C.P.; Umar, A. Hierarchical porous carbon aerogel derived from bagasse for high performance supercapacitor electrode. *Nanoscale* **2014**, *6*, 12120–12129. [[CrossRef](#)] [[PubMed](#)]
64. Basnayaka, P.A.; Ram, M.K.; Stefanakos, L.; Kumar, A. Graphene/Polypyrrole Nanocomposite as Electrochemical Supercapacitor Electrode: Electrochemical Impedance Studies. *Graphene* **2013**, *2*, 81–87. [[CrossRef](#)]
65. Papon, E.A.; Haque, A.; Spear, S.K. Effects of functionalization and annealing in enhancing the interfacial bonding and mechanical properties of 3D printed fiber-reinforced composites. *Mater. Today Commun.* **2020**, *25*, 101365. [[CrossRef](#)]
66. Kim, B.K.; Sy, S.; Yu, A.; Zhang, J. Electrochemical Supercapacitors for Energy Storage and Conversion. In *Handbook of Clean Energy Systems*; John Wiley and Sons: Hoboken, NJ, USA, 2015; pp. 1–25. [[CrossRef](#)]
67. Karnan, M.; Raj, A.G.K.; Subramani, K.; Santhoshkumar, S.; Sathish, M. The fascinating supercapacitive performance of activated carbon electrodes with enhanced energy density in multifarious electrolytes. *Sustain. Energy Fuels* **2020**, *4*, 3029–3041. [[CrossRef](#)]

Disclaimer/Publisher’s Note: The statements, opinions and data contained in all publications are solely those of the individual author(s) and contributor(s) and not of MDPI and/or the editor(s). MDPI and/or the editor(s) disclaim responsibility for any injury to people or property resulting from any ideas, methods, instructions or products referred to in the content.